# CO2 solubility and diffusivity in 1-ethyl-3-methylimidazolium cation-based ionic liquids; isochoric pressure drop approach

Qazi Sohaib, Mohammad Amin Kazemi, Christophe Charmette, Jim Cartier, Mohammad Younas, Abouzar Azarafza, Mashallah Rezakazemi, José Sanchez-Marcano

# $CO_2$ solubility and diffusivity in 1-ethyl-3-methylimidazolium cation-based ionic liquids; isochoric pressure drop approach

Qazi Sohaib[1], Mohammad Amin Kazemi[2], Christophe Charmette[1], Jim Cartier[1], Mohammad Younas[3], Abouzar Azarafza[4], Mashallah Rezakazemi[5,*], José Sanchez-Marcano[1]

[1] *Institut Européen des Membranes, IEM, Université de Montpellier, CNRS, ENSCM, 34090 Montpellier, France*

[2] *Department of Mechanical and Industrial Engineering, University of Toronto, Toronto, ON, Canada M5S 3G8*

[3] *Department of Chemical Engineering, Faculty of Mechanical, Chemical and Industrial Engineering, University of Engineering and Technology, Peshawar 25120, Pakistan*

[4] *School of Chemical and Biomedical Engineering, Department of Chemical Engineering, The University of Melbourne, Parkville, Victoria 3010, Australia*

[5] *Faculty of Chemical and Materials Engineering, Shahrood University of Technology, Shahrood, Iran*

*Corresponding Author Email: mashalah.rezakazemi@gmail.com (M. Rezakazemi)*

**Abstract**

In this study, an experimental approach based on the isochoric pressure drop principle was implemented to measure (at low equilibrium pressure, 1.3-3.6 bar) the solubility and binary diffusivity of $CO_2$ (constant and variable) in four imidazolium-based room-temperature ionic liquids (RTILs), namely, 1-ethyl-3-methylimidazolium acetate ([emim][Ac]), 1-ethyl-3-methylimidazolium dicyanamide ([emim][DCA]), 1-ethyl-3-methylimidazolium methyl sulfate ([emim][$MeSO_4$]) and 1-ethyl-3-methylimidazolium ethyl sulfate ([emim][$EtSO_4$]). The molar fraction of the dissolved $CO_2$ and Henry's law constant were measured from experimental data. Constant binary diffusion coefficients were measured from the transient thin-film and semi-infinite volume models. In the original approach, the variable diffusivity coefficient model was used to measure the concentration-based variable diffusion coefficient. Anion interaction of the RTILs was found to have a strong influence on the $CO_2$ solubility, and Henry's law constant and the studied anions were ranked as $[Ac]^- >> [EtSO_4]^- > [DCA]^- > [MeSO_4]^-$. Increasing temperature is not likely for $CO_2$ solubility while it favors $CO_2$ diffusivity. Thin-film model diffusivity measurements were found to be more suitable for [emim][$MeSO_4$] and [emim][$EtSO_4$], while semi-infinite volume model was suitable for [emim][Ac] and [emim][DCA]. Variable diffusion coefficients were found not to be a monotonous function of time, which increased in early stages and decreased after a certain time. Gibbs free energy, enthalpy, and entropy values indicate the strength of the favorable interaction between $CO_2$ and RTILs, mildly exothermic in nature and falling in the range of physisorption.

**Keywords:** $CO_2$ Solubility, $CO_2$ Diffusion Coefficients, Room Temperature Ionic Liquids (RTILs), Transient Thin-Film Model, Semi-Infinite Volume Model, Variable Diffusivity Coefficient Model

## 1 Introduction

Carbon capture technologies are attracting the attention of governments and scientists due to the significant contribution of carbon dioxide ($CO_2$) to greenhouse gases [1]. This high $CO_2$ concentration makes it a leading cause of climatic disturbances, including notable ones as high earth surface temperature and global warming [2]. Among different technologies, carbon capture based on liquid absorbents like aqueous alkanolamines has high $CO_2$ removal efficiency (> 80%) even at low pressures and $CO_2$ concentrations [3] and is relatively inexpensive [4,5]. Although these absorbents are very efficient on an industrial scale, they face serious problems, including substantial energy consumption, the release of toxic by-products to the environment due to their volatile nature, operational instability, excessive corrosion, and frequent equipment maintenance [4,6]. Consequently, the discovery of alternative absorbents, which could effectively absorb $CO_2$ and simultaneously overcome the aforementioned problems, is significant.

Ionic Liquids (ILs) provide an attractive and promising alternative to actual aqueous alkanolamines for $CO_2$ capture [7,8]. ILs are organic salts with organic cation and an organic or inorganic anion, with a melting point mostly lower than 100 °C. Unique properties such as high $CO_2$ solubility, negligible vapor pressure and volatility, and high thermal stability make them very attractive to conventional organic solvents [9,10]. Due to their unique physicochemical properties and tunable molecular structures, ILs are also known as designer solvents [4]. ILs have been categorized as room temperature ionic liquids (RTILs) and functionalized or task-specific ionic liquids (TSILs) [11]. Both ILs provide high $CO_2$ solubility; however, TSILs can provide higher solubility (up to 3 folds) than RTILs. RTILs have been mostly observed to provide only physisorption, while TSILs can provide both chemisorption and physisorption [12]. Due to chemisorption, TSILs can absorb $CO_2$ even at very low partial pressure values [13].

Conventional ILs mostly follow the physical absorption mechanism (no chemical reaction) [14]. Anions and cations play a vital role in the sorption of $CO_2$ in ILs. Anions are believed to play a primary role, while cations indirectly impact sorption. Various experimental and simulation reports have found similar effects [15–17]. Various studies have claimed that $CO_2$ solubility in ILs relies not solely on the anion-cation interaction mechanism but also on the free volume mechanism [14]. In this mechanism, a $CO_2$ molecule is captured by the absorbent in the available free space, while there is no change in the total volume of the absorbent, even after absorbing a large amount of $CO_2$ [18,19]. TSILs developed for $CO_2$ capture include protic ILs [20], amine-based ILs [21], and amino acid-based ILs [22]. The absorption mechanism of the TSILs depends on whether the IL is cation functionalized or anion functionalized.

The potential applicability of the ILs on an industrial scale requires the knowledge of important features, including solubility and solubility rate, i.e., diffusivity [23]. Various methods have been implemented to determine the experimental gas/liquid solubilities and Henry's law constants. These methods include gravimetric microbalance method [17,24], NMR spectroscopy [25], optical methods [26] and time lag method [27]. All the methods mentioned above experience some serious drawbacks. Another method known as the pressure drop method has been implemented by various researchers [28,29]. In this method, a defined volume of gas is brought in contact with a known volume of IL in a closed chamber at a constant temperature. The pressure drop due to sorption is monitored and further used for calculations [30]. Young *et al.* [31] mentioned various indirect methods to measure gas diffusion coefficients, including pressure drop/decay method [32,33], electromagnetic method [34], pH method [35], visualized dye method [31], density methods [36] and swelling pendant droplet method [37]. Among these methods, the pressure drop/decay method

is regarded as one of the most common methods for measuring gas diffusivity due to its simple experimental approach and wide pressure range applicability [31].

In the past, various researchers have reported the solubility and diffusivity data for different ILs. However, there is still a huge gap due to the availability of many ILs and their different combinations. Afzal *et al.* [38] reported $CO_2$ solubility of imidazolium-based ILs, namely, l-n-butyl-3-methylimidazolium tetrafluoroborate [bmim][$BF_4$], l-n-butyl-3-methylimidazolium hexafluorophosphate [bmim][$PF_6$], 1-ethyl-3-methylimidazolium bis (trifluoromethyl sulfonyl) imide [emim] [$Tf_2N$], and 1-ethyl-3-methylimidazolium acetate [emim][Ac]. Shokouhi *et al.* [39] implemented semi-infinite volume method to measure diffusion coefficients of $CO_2$ in IL 1-Ethyl-3-methylimidazoliumtris (pentafluoroethyl) trifluorophosphate [emim][eFPT], [emim] [$Tf_2N$], 1-(2-hydroxyethyl)-3-methylimidazolium trifluoromethanesulfonate [hemim][OTf], 1-(2-hydroxyethyl)-3-methylimidazolium hexafluorophosphate [hemim][PF6], 1-(2-hydroxyethyl)-3-methylimidazolium bis-(trifluoromethyl) sulfonylimide [hemim][$NTf_2$]. The authors observed an increase in the diffusivity of $CO_2$ with an increase in the temperature. The diffusivity was greater in [emim] based ILs than in [hemim] based. Morgan *et al.* [40] developed a correlation to predict the diffusivity of $CO_2$ in imidazolium-based RTILs, using a time lag technique. The correlation strongly depends on the RTILs diffusion coefficients on the viscosity. Hou and Baltus [41] developed another correlation for $CO_2$ diffusivity in RTILs based on the transient thin-liquid-film method. They reported the dependency of $CO_2$ diffusion coefficients on the anion and cation of ILs. The result showed that the $CO_2$ diffusivity is more temperature-sensitive than the $CO_2$ solubility.

This work is focused on the measurement of the solubilities and binary diffusion coefficients of four imidazolium-based ILs, 1-ethyl-3-methylimidazolium acetate ([emim][Ac]), 1-ethyl-3-

methylimidazolium dicyanamide ([emim][DCA]), 1-ethyl-3-methylimidazolium methyl sulfate ([emim][$MeSO_4$]), 1-ethyl-3-methylimidazolium ethyl sulfate ([emim][$EtSO_4$]). The work here adopts an isochoric pressure drop method to measure the solubility of $CO_2$ in the studied ILs. In each experiment, the diffusion was allowed to reach equilibrium, which measured Henry's law constant. To calculate the diffusion coefficients from the experimental data, the diffusion of $CO_2$ in the ILs is expressed by three mathematical models, namely, transient thin-film method, semi-infinite volume method, and variable diffusivity coefficient method. These methods are deeply studied, and the obtained diffusion coefficients are compared with those predicted by the correlations developed by Morgan *et al.* [40] and Hoe and Baltus [41]. The study is further extended to determine the Gibbs free energy, enthalpy, and entropy of the solution.

## 2 Materials and methods

### 2.1 Materials and characterization

Analytical grade $CO_2$ (Purity ≥ 99,9995 % vol) was provided by Linde, France. Four different imidazolium based RTILs, 1-ethyl-3-methylimidazolium acetate ([emim][Ac]), 1-ethyl-3-methylimidazolium dicyanamide ([emim][DCA]), 1-ethyl-3-methylimidazolium methyl sulfate ([emim][$MeSO_4$]), 1-ethyl-3-methylimidazolium ethyl sulfate ([emim][$EtSO_4$]) with purities greater than 95 % were purchased from Sigma-Aldrich. Some basic information and physical properties of the RTILs are presented in Table 1 and Table 2, below.

**Table 1** Ionic liquids basic information

| S. No | IL | Molecular formula | Supplier/ source | CAS Number | Water contents (%)[a] | Purity[b] | MW (g $mol^{-1}$) |
|---|---|---|---|---|---|---|---|
| **1** | [emim][Ac] | $C_8H_{14}N_2O_2$ | Sigma-Aldrich | 143314-17-4 | ≤ 1.0 | 0.990 | 170.21 |
| **2** | [emim][DCA] | $C_8H_{11}N_5$ | Sigma-Aldrich | 370865-89-7 | ≤ 0.50 | 0.995 | 177.21 |

| | | | | | | | |
|---|---|---|---|---|---|---|---|
| **3** | [emim][$MeSO_4$] | $C_7H_{14}N_2O_4S$ | Sigma-Aldrich | 516474-01-4 | ≤ 0.2 | 0.998 | 222.26 |
| **4** | [emim][$EtSO_4$] | $C_8H_{16}N_2O_4S$ | Sigma-Aldrich | 342573-75-5 | ≤ 2.0 | 0.980 | 236.29 |

[a] mass %, [a,b] from supplier, no further water removal or purification performed

**Table 2** Basic properties of the ionic liquids

| **S. No** | **IL** | **Density[a] ($g\ m^{-3}$)** | **Viscosity[b] (mPa s)** | **Surface tension[c] ($mN\ m^{-1}$)** | |
|---|---|---|---|---|---|
| | | | | This Work | Literature [d] |
| **1** | [emim][Ac] | 1.099 | 141.1 | 46.8 | 47.1 |
| **2** | [emim][DCA] | 1.108 | 15.1 | 45.4 | 44.1, 42.6 |
| **3** | [emim][$MeSO_4$] | 1.286 | 78.1 | 51.2 | 52.6, 52.5 |
| **4** | [emim][$EtSO_4$] | 1.237 | 97.0 | 46.3 | 47.2 |

[a,b] at 298.15 K [42–46]; [c] at 298.15 K; [d] [47–52]

$CO_2$, Nitrogen ($N_2$) (99.7 % ±0.01 vol%), and Helium (He) (99.9 % ±0.001 vol%) gases were purchased from Linde France. The surface tension of the imidazolium-based RTILs was measured using a Langmuir device (KSV NIMA Langmuir-Blodgett) which employs a Wilhelmy plate made of platinum partially immersed in the IL. The apparatus allows determining the surface tension using the Wilhelmy plate method. A thermogravimetric and differential thermal analyzer (Shimadzu, DTG-60) was used to analyze the thermal stability of RTILs. Samples of IL were analyzed with a heating rate of 5 $^oC\ min^{-1}$ in the presence of $N_2$ flowing at 50 ml $min^{-1}$.

## 2.2 Experimental setup

Equilibrium solubilities of $CO_2$ in RTILs were measured with the help of the isochoric pressure drop principle using an IEM-built (Institut Européen des Membranes) apparatus, which is presented schematically in Figure 1. The $CO_2$ solubility measurements were performed at different temperatures and pressures.

The temperature of the apparatus was controlled and kept constant by keeping it in a temperature-controlled chamber (Sartorius Certomat HK). The apparatus could perform two measurements simultaneously (two equilibrium cells). Each of the equilibrium cells was sealed with a copper gasket. Equilibrium cells were connected to a secondary reservoir used for the gas injection. The primary reservoir, made up of stainless steel, provided gas to each secondary reservoir. Pressure and temperature values of the equilibrium cells and primary reservoir were monitored by exact (0.01%) pressure sensors (KELLER, PA33X). The pressure sensors were connected to a data acquisition system, and the collected data were stored in a computer for further processing.

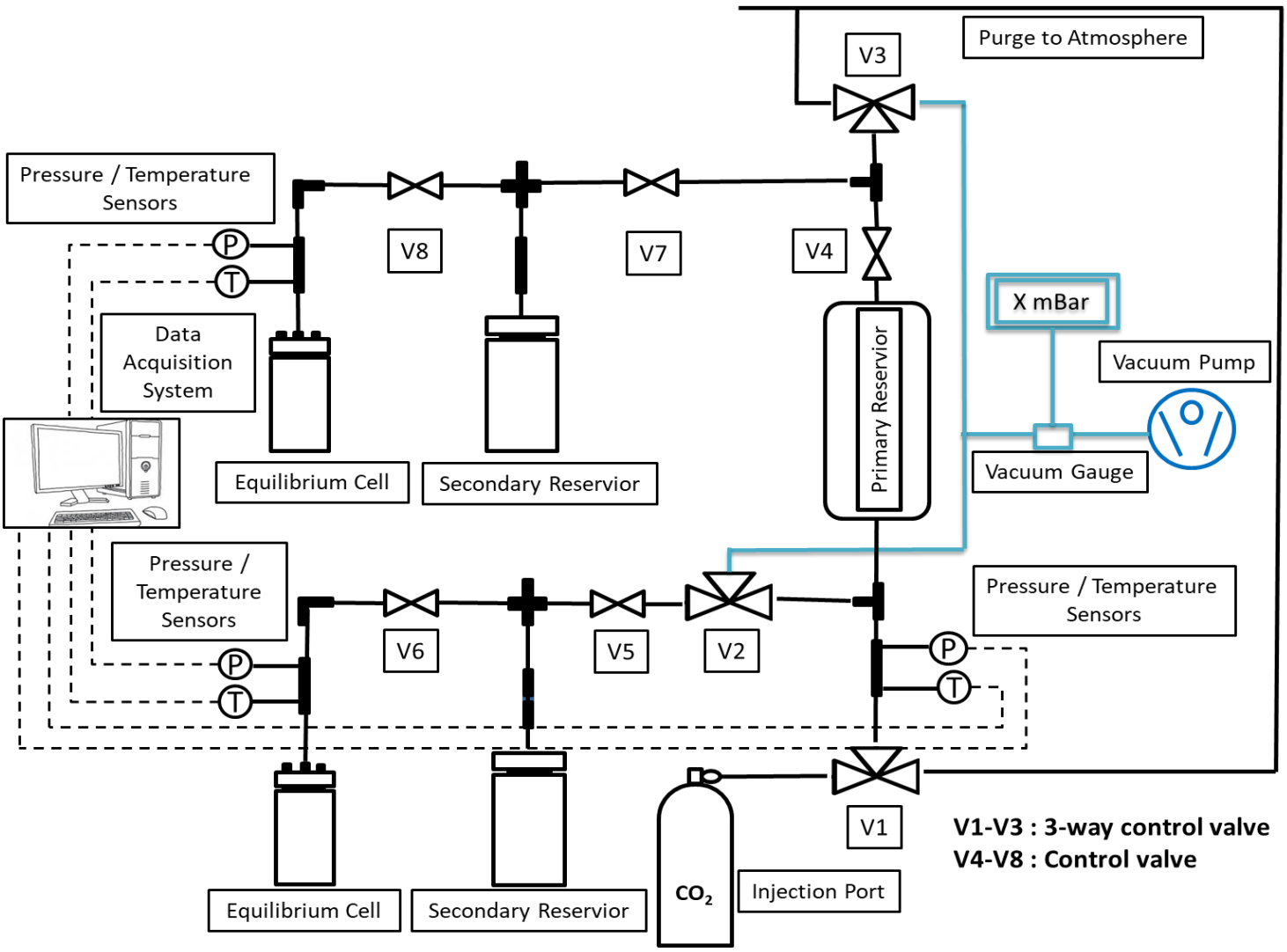


**Figure 1** Schematic representation of the experimental setup used for gas solubility and diffusivity measurements based on the isochoric pressure drop principle.

Before each experiment, the setup was checked for possible leakage by filling it with He gas and using a leak detector (Alcatel ASM series). The volume of each apparatus section was measured using He gas, assuming the ideal gas law. IL of known volume (5 ml) was added to each equilibrium cell and sealed using a copper gasket for experimentation. The available volumes for the gas in equilibrium cells 1 and 2 were 0.19285 and 0.19631 L, respectively. The equilibrium cells were cylindrical and therefore, the 5 mL IL formed a surface area of 7.06 $cm^{2,}$ and the thickness of the liquid film was calculated to be $L$ = 7.08215 mm. The equilibrium cells were then

put on the degassing and/or desorption mode by applying a vacuum pressure of $5 \times 10^{-5}$ mbar for 10 h. After degassing, the $CO_2$ was transferred to the primary reservoir and then to the secondary reservoirs. The gas was allowed to expand in the secondary reservoirs for 30 min to ensure the homogeneity of pressure and temperature of the gas before introducing it to the equilibrium cell. Finally, secondary reservoir 1 and secondary reservoir 2 were connected to equilibrium cell 1 and 2, respectively, and the gas was allowed to be absorbed in the IL in the equilibrium cells. Once the experiment was started, the gradual pressure drop could be observed from the collected data by the data acquisition system.

## 3 Theoretical analysis

The pressure drop in the gas phase was recorded in each experiment. The amount of $CO_2$ absorbed in the IL was calculated using the conservation of mass and the ideal gas law:

$$N_{CO_2} = \frac{\Delta P\, V}{R\, T} \tag{1}$$

where $N_{CO_2}$ is the molar amount of $CO_2$ absorbed at equilibrium, $\Delta P$ (bar) represents the pressure difference between the initial pressure ($P_0$) and equilibrium state pressure ($P_\infty$) of the equilibrium cell, $V$ represents the volume of the gas which is found by subtracting the IL volume from the volume of the empty equilibrium cell, $T$ is the equilibrium temperature, and $R$ is the ideal gas constant. The molar composition of the absorbed $CO_2$ gas in the liquid can be found as follows:

$$x_{CO_2} = \frac{N_{CO_2}}{N_{CO_2} + N_{IL}} \tag{2}$$

where $N_{IL}$ represents the number of moles of IL used.

Henry's law constant $K_H$ (bar) can be calculated from the recorded equilibrium pressure $P_\infty$ and the corresponding molar fraction of the $CO_2$ in the liquid phase:

$$K_H = \frac{P_\infty}{x_g} \tag{3}$$

The binary diffusion coefficients of $CO_2$ into the ILs may be determined using the existing theories. Two commonly used mathematical models in the literature can be employed to calculate the diffusivity coefficients. While both methods utilize Fick's second law of diffusion, they use different assumptions at the liquid boundaries. Here we provide a brief overview of both models and their governing equations. Note that the analytical solutions based on these approaches are available only when the diffusivity coefficient is taken to be independent of the concentration. In the case of a variable diffusivity coefficient, the solution becomes complex and needs to be solved numerically. As a result, the third model studied here is devoted to the numerical solution to Fick's second law with a variable diffusion coefficient. The binary diffusion coefficients are obtained by fitting the model predictions of the instantaneous pressures of the gas phase to the measured pressures. The binary diffusion coefficients obtained from these three methods are compared together.

### 3.1 Model 1-Transient thin-film method

The mathematical model representing the diffusion of $CO_2$ into the thin liquid film of the IL is described in this section. In this model, it is considered a film of liquid placed in between a gas and a solid phase. The diffusion coefficients are determined by applying a mass diffusion model proposed by Shifflet and Yokoezi [53]. For the diffusion of a gas into a thin liquid film, Hou and Baltus [41] provided an analytical solution for the concentration profile of the dissolved gas in the liquid by coupling the diffusion equation with the pressure drop equation in the adjacent gas. For

simplicity, it is assumed that the diffusion of $CO_2$ in the liquid takes place in one dimension, from the liquid-gas interface to a solid boundary. Besides, the liquid is assumed to be quiescent, meaning there is no convective transport of $CO_2$ in the liquid phase. The partial pressure of the IL in the gas phase is assumed to be negligible due to the low vapor pressure of the IL. The molecular diffusion is assumed to occur slowly enough to establish chemical equilibrium at the liquid-gas boundary. Under these assumptions, the component mass balance for $CO_2$ in the liquid phase reduces to Fick's second law:

$$\frac{\partial c}{\partial t} = D\frac{\partial^2 c}{\partial z^2} \tag{4}$$

where $c$ is the molar concentration of $CO_2$ in the liquid, $t$ is time, $D$ is the diffusion coefficient, and $z$ is the vertical direction. The system geometry is defined such that $z = 0$ corresponds to the base of the liquid film and $z = L$ corresponds to the liquid-gas interface. The diffusivity coefficient is assumed to be independent of the concentration. The gas phase is assumed to have a uniform temperature and pressure. Assuming the ideal gas law, the mass balance in the gas phase is given by:

$$\frac{\mathrm{d}P}{\mathrm{d}t} = \frac{RT}{V}\frac{\mathrm{d}N}{\mathrm{d}t} = \frac{RT}{V}\left(\frac{V_{\mathrm{IL}}}{L}\right)\left(-D\frac{\partial c}{\partial z}\Big|_{z=L}\right) \tag{5}$$

where $V$ is the volume of the gas in the chamber, $N$ is the number of moles of $CO_2$ in the gas, and $V_{\mathrm{IL}}$is the volume of the IL. Both $V$ and $V_{\mathrm{IL}}$ are taken constantly. Initially, the concentration of $CO_2$ in the liquid is zero, and the initial pressure in the gas ($P_0$) is known.

$$P(0) = P_0, \qquad c(z,0) = 0 \tag{6}$$

It is assumed that $CO_2$ molecules do not penetrate the base solid. Therefore, at $z = 0$:

$$t > 0, \qquad \left.\frac{\partial c}{\partial z}\right|_{z=0} = 0 \tag{7}$$

At the liquid-gas boundary, local equilibrium is assumed to exist. Therefore, the pressure in the gas phase may be related to the concentration in the liquid phase using Henry's law:

$$c(L,t) = \frac{\rho_{\mathrm{IL}}}{K_H\, M_{\mathrm{IL}}} P(t); \tag{8}$$

where $\rho_{\mathrm{IL}}$ is the density of the liquid, $K_H$ is Henry's law constant, and $M_{\mathrm{IL}}$ is the molar mass of the IL. Eqs. 4-8 may be combined to obtain the concentration in the liquid [41]:

$$\frac{c(z,t)}{c(L,t)} = 1 - \left(\frac{4}{\pi}\right)\sum_{n=0}^{\infty}\frac{(-1)^n}{(2n+1)}\cos\left(\frac{(2n+1)\pi z}{2L}\right)\exp\left(\frac{-(2n+1)^2\pi^2 Dt}{4L^2}\right) \tag{9}$$

By making use of Eq.9 and integrating Eq. 5 from $t$ = 0 to an arbitrary $t$, the concentration is eliminated, and the pressure decay in the gas phase may be expressed as a function of the fluid properties and system parameters [41]:

$$\ln\frac{P(t)}{P_0} = \left(\frac{8RTV_{\mathrm{IL}}\rho_{\mathrm{IL}}}{\pi^2 K_H V M_{\mathrm{IL}}}\right)\sum_{n=0}^{\infty}\frac{-1}{(2n+1)^2}\left[1 - \exp\left(\frac{-(2n+1)^2\pi^2 Dt}{4L^2}\right)\right] \tag{10}$$

In each experiment, the instantaneous pressure in the gas phase was recorded. Therefore, by fitting Eq. 10 to the experimental pressures, the value of $D$ can be determined.

### 3.2 Model 2-Semi-infinite volume method

In this model, the liquid film is assumed to be thick enough to be considered a semi-infinite domain. Given that the concentration has a finite value at infinity, the solution to eq. 4 becomes:

$$c(x,t) = c(0,0)\mathrm{erfc}\left(\frac{x}{2\sqrt{Dt}}\right) + k\sqrt{\pi t}\,\mathrm{ierfc}\left(\frac{x}{2\sqrt{Dt}}\right) \tag{11}$$

where $k$ is a constant with respect to $t$ and $x$. The function "ierfc" is the integral of the complementary error function and is given by:

$$\text{ierfc}(u) = u\,\text{erfc}(u) - \frac{1}{\sqrt{\pi}} e^{-u^2} \tag{12}$$

At the liquid-gas interface ($x$ = 0), the concentration is proportional to the square root of time:

$$c(0,t) = c(0,0) - k\sqrt{t} \tag{13}$$

The boundary condition in Eq. 13 can be obtained from Eq. 11 by setting $x$=0. The constant $k$ should be determined by fitting the best line to the plot of $c$ with $t^{1/2}$. The mole flux of diffusion at the liquid-gas boundary is:

$$-D\left.\frac{\partial c}{\partial x}\right|_{x=0} = c(0,0)\frac{1}{\sqrt{\pi D t}} - \frac{k}{2}\sqrt{\frac{\pi}{D}} \tag{14}$$

Finally, the cumulative gas that has diffused into the semi-infinite volume at time $t$ may be calculated by:

$$M_t = \int_0^t \left(-D\left.\frac{\partial c}{\partial x}\right|_{x=0}\right) \mathrm{d}t = \sqrt{D}\left[2c(0,0)\sqrt{\frac{t}{\pi}} - \frac{1}{2}kt\sqrt{\pi}\right] \tag{15}$$

$M_t$ is the number of moles of $CO_2$ that have diffused in the liquid.

### 3.3 Model 3-Variable diffusivity coefficient

In the third model, Fick's second law equation is solved, assuming that the diffusivity coefficient is variable during the diffusion process. Therefore:

$$\frac{\partial c}{\partial t} = \frac{\partial}{\partial z}\left(D\frac{\partial c}{\partial z}\right) \tag{16}$$

The diffusivity coefficient is taken as an adjusting parameter determined by fitting the numerical solution of eq.16 to the experimental pressure decay data obtained in each experiment. Since it is difficult to calculate *D* with time, a PID controller equation is coupled to the system of equations to automatically adjust *D* and ensure that the numerical solution closely follows the experimental data. The equation for a PID controller is:

$$D(t) = K_p e(t) + K_i \int_0^t e(\tau)\,\mathrm{d}\tau + K_d \frac{\mathrm{d}e(t)}{\mathrm{dt}} \tag{17}$$

where $e(t)$ is the error which is defined as the difference between the calculated and the experimental pressures:

$$e(t) = P(t) - P_{\mathrm{exp}}(t) \tag{18}$$

The constants $K_p$, $K_i$, and $K_d$ are the controller parameters determined such that the simulated pressures are very close to the experimental data. Note that we are not interested in obtaining the best controller parameters, and any combination of $K_p$, $K_i$, and $K_d$ that leads to calculating the pressure values which are close enough to the measured pressures would be acceptable.

## 4 Results and discussion

The thermal stability of ILs is an important parameter while considering $CO_2$ sorption. An increase in temperature significantly affects the solubility of $CO_2$ in ILs. Generally, an increase in temperature decreases the $CO_2$ solubility in the RTILs. An increase in temperature also affects the viscosity of the ILs, thus affecting the Diffusion coefficients. Therefore, a thermal stability analysis was conducted using TGA analysis. Samples were heated from 18 to 450 $^{o}$C. Figure 2 confirms that all IL's were thermally stable for the temperature range studied (303.15-333.15 K). IL [emim][$MeSO_4$], [emim][DCA] and [emim][EtSO4] have only 4% of weight loss until 473.15,

543.15 and 573.15 K. IL [emim][Ac] loses only 2 % weight until 473.15 K. The initial minor losses can be attributed to water loss from the samples. In conclusion, all four ILs are stable for use at temperatures below 473.15 K.

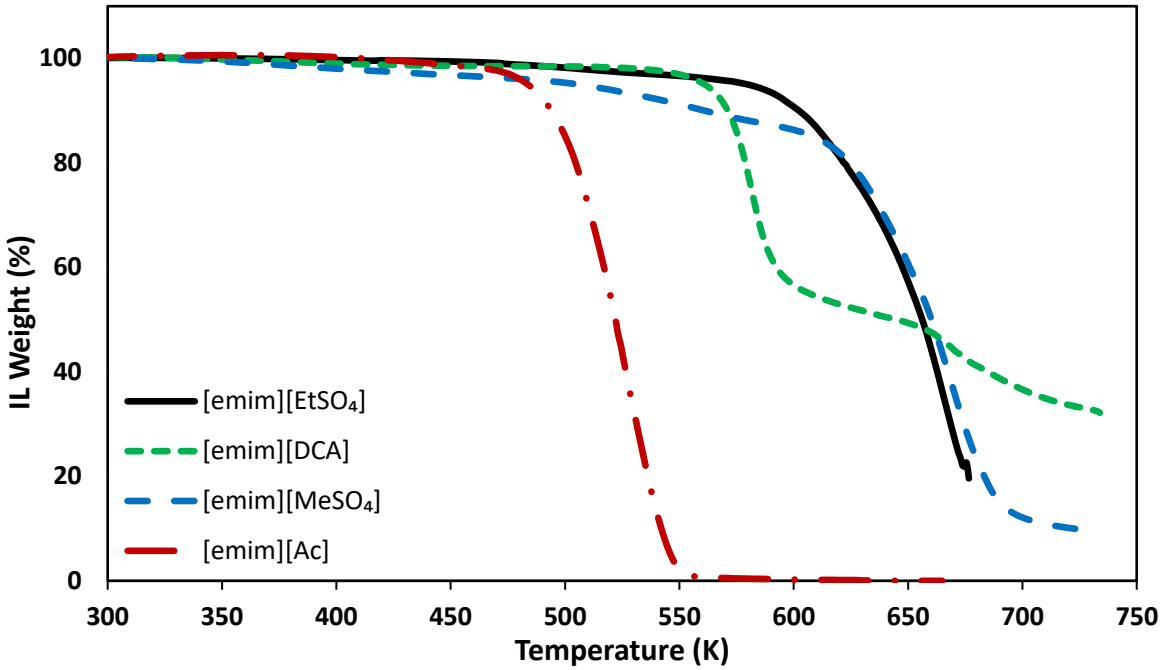


**Figure 2** TGA analysis of ILs [12]

ILs can be characterized for $CO_2$ sorption capacity by measuring $CO_2$ solubility and Henry's law constant. A low Henry's law constant value indicates a high gas solubility [54]. Experimental solubilities were measured using the isochoric pressure drop principle method (Figure 1) and corresponding Henry's law constants (determined from the solubility data using Eqs.1–3) of $CO_2$ in four RTILs are presented in Table 3. In Table 3, $P_0$ is the initial pressure and $P_\infty$ is the equilibrium state pressure in the gas phase. The amount of IL (moles) used in each experiment is also listed. The data of the instantaneous pressures with time for each IL is provided in the supplementary information. A complete list of variables is provided in the Nomenclature. Solubilities are presented in the form of the molar fraction of $CO_2$, $x_{CO_2}$, while Henry's law

constants ($K_H$) are presented in bar. The uncertainties associated with each parameter are computed using propagation of uncertainty. The equations for calculating the uncertainties are provided in supporting information (Eq. S1-S3). For the pressure, the uncertainty is taken ±0.1% of the transducer full scale (0-10 bar). For the temperature, it is taken ±0.05 °C which is the maximum error of the calibration.

**Table 3** Experimental solubilities and Henry' law constants of $CO_2$ in different ILs

| IL | $T$ (K) | $P_0$ (bar) | $P_\infty$ (bar) | Amount of IL (mole) | $x_{CO_2}$ | $K_H = P_\infty / x_{CO_2}$ (bar) |
|---|---|---|---|---|---|---|
| **[emim][Ac]** | 303.1±0.05 | 2.596±0.003 | 1.343±0.001 | 0.032298 | 0.2341±0.0005 | 5.7±0.02 |
| | 302.1±0.05 | 3.582±0.004 | 2.104±0.002 | 0.032298 | 0.2618±0.0006 | 8.0±0.03 |
| | 313.2±0.05 | 3.558±0.004 | 2.254±0.002 | 0.032116 | 0.2261±0.0005 | 10.0±0.03 |
| | 323.2±0.05 | 3.555±0.004 | 2.385±0.002 | 0.031936 | 0.2119±0.0005 | 11.2±0.04 |
| | 333.2±0.05 | 3.583±0.004 | 2.523±0.003 | 0.031936 | 0.1941±0.0001 | 12.9±0.04 |
| **[emim][DCA]** | 303.6±0.05 | 2.166±0.002 | 2.073±0.002 | 0.031304 | 0.0221±0.0001 | 96.6±0.3 |
| | 303.6±0.05 | 2.622±0.003 | 2.543±0.003 | 0.031304 | 0.0222±0.0001 | 108.8±0.4 |
| | 303.2±0.05 | 3.603±0.004 | 3.483±0.003 | 0.031304 | 0.0229±0.0001 | 152.1±0.5 |
| | 313.9±0.05 | 3.592±0.004 | 3.437±0.003 | 0.030850 | 0.0367±0.0001 | 92.9±0.3 |
| | 322.7±0.05 | 3.590±0.004 | 3.501±0.004 | 0.030666 | 0.0253±0.0001 | 136.0±0.5 |
| | 332.6±0.05 | 3.604±0.004 | 3.541±0.004 | 0.030484 | 0.0237±0.0001 | 132.4±0.4 |
| **[emim][MeSO$_4$]** | 304.5±0.05 | 2.712±0.003 | 2.593±0.003 | 0.028899 | 0.0336±0.0000 | 77.2±0.3 |
| | 304.9±0.05 | 2.239±0.003 | 2.161±0.003 | 0.028899 | 0.0169±0.0001 | 128.2±0.4 |
| | 304.0±0.05 | 2.670±0.003 | 2.587±0.003 | 0.028899 | 0.0237±0.0001 | 104.6±0.4 |
| | 314.0±0.05 | 3.685±0.004 | 3.560±0.004 | 0.031682 | 0.0313±0.0000 | 112.5±0.4 |
| | 322.5±0.05 | 3.676±0.004 | 3.603±0.004 | 0.028549 | 0.0188±0.0000 | 188.2±0.6 |
| | 332.0±0.05 | 3.669±0.004 | 3.625±0.004 | 0.028399 | 0.0210±0.0001 | 149.0±0.5 |
| **[emim][EtSO$_4$]** | 303.9±0.05 | 2.689±0.003 | 2.555±0.003 | 0.026144 | 0.0408±0.0001 | 59.9±0.2 |
| | 303.1±0.05 | 3.691±0.004 | 3.470±0.003 | 0.026144 | 0.0594±0.0001 | 58.9±0.2 |
| | 315.1±0.05 | 3.684±0.004 | 3.520±0.004 | 0.025953 | 0.0493±0.0001 | 68.8±0.2 |
| | 324.4±0.05 | 3.704±0.004 | 3.562±0.004 | 0.025805 | 0.0431±0.0001 | 79.0±0.3 |
| | 332.5±0.05 | 3.696±0.004 | 3.602±0.004 | 0.025699 | 0.0263±0.0001 | 133.1±0.4 |

It can be observed from Table 3 that the solubility of $CO_2$ in the studied RTILs decreases with temperature. For example, for the same initial pressure ($P_0$), the $CO_2$ mole fraction in [emim][Ac] decreased from 0.2617 to 0.1941 as the temperature increased from 302.75 to 333.15 K. Henry's law constants are also temperature dependent. For example, in the case of [emim][Ac], the Henry's law constant increased from 8.03 to 12.94 bar as the temperature increased from 302.75 to 333.15

K, while the initial pressure is the same for these two experiments. An increase in the $K_H$ values means a decrease in solubility. Similar effects of a decrease in the $CO_2$ solubility and an increase in Henry's law constant with temperature enhancement are observed in other studies (Table 4). Table 4 summarizes data in the literature for $CO_2$ solubility in the studied ILs. For example, in the case of IL [emim][$EtSO_4$] at 303.15 K, the $x_{CO_2}$ value reported by Jalili et al. [55] is 0.047 and the one reported by Soriano et al. [56] is 0.031, while the one measured in this study at 303.9 K is 0.0408.

**Table 4** Solubilities and Henry' law constants of $CO_2$ in the studied ILs from different literature

| ILs | T (K) | P (bar) | $x_{CO_2}$ | $K_H = P_\infty / x_{CO_2}$ (bar) | Ref. |
|---|---|---|---|---|---|
| **[emim][Ac]** | 298.15 | 2.54 | 0.3080 | - | [57] |
| | 348.15 | 2.55 | 0.2110 | - | [57] |
| | 333.15 | 1.88 | 0.2200 | 8.33 | [58] |
| **[emim][DCA]** | 298.20 | 3.03 | 0.0298 | 101.00 | [59] |
| | 313.20 | 3.05 | 0.0249 | 146.00 | [59] |
| | 333.20 | 3.02 | 0.0169 | 200.00 | [59] |
| | 313.15 | - | - | 95.90 | [60] |
| **[emim][$MeSO_4$]** | 303.15 | 6.30 | 0.0890 | - | [61] |
| | 298.15 | - | - | 130.00 | [62] |
| | 313.15 | - | - | 170.00 | [62] |
| | 328.15 | - | - | 220.00 | [62] |
| **[emim][$EtSO_4$]** | 303.15 | 4.69 | 0.047 | 97.80 | [55] |
| | 313.15 | 4.91 | 0.043 | 111.00 | [55] |
| | 303.15 | 2.11 | 0.031 | - | [56] |

The magnitude of $K_H$ value can indicate whether the absorption is chemisorption ($K_H$ <30 bar) or physisorption ($K_H$ >30 bar) [63][64]. According to this condition, the $K_H$ values listed in Table 3 show that the $CO_2$ absorption with [emim][$MeSO_4$], [emim][DCA] and [emim][$EtSO_4$] is physisorption, while with [emim][Ac] it's chemisorption. This phenomenon of solubility decrease and Henry's law constant increase with an increase in temperature can also be confirmed by Zubeir

et al. [65] and Blath et al. [30], who studied the effect of temperature on the $CO_2$ solubility of RTILs.

Various authors (from experimental findings and simulations) have reported the effect of cation and anion of an IL over the $CO_2$ solubility; however, the anion is believed to have a greater impact than cation. In the current study, we only changed the anions and kept one cation, which is an imidazolium-based cation (1-ethyl-3-methylimidazolium, $[emim]^+$) for all ILs. Table 3 confirms the evident effect of ILs anion on the $CO_2$ solubility. We can observe from the results that acetate $[Ac]^-$ anion provides very high $CO_2$ solubility in combination with $[emim]^+$ cation, compared to other anions of this study. Based on the findings of this study, in terms of $CO_2$ solubility, these ILs can be ranked as [emim][Ac] >> [emim][$EtSO_4$] > [emim] [DCA] > [emim][$MeSO_4$].

The experimental data of the pressure decay with time were fit to the proposed models (Eqs.10, 15, and 16) using a custom code written in MATLAB, and the diffusion coefficients (*D*) were determined. The temperature-dependent densities and viscosities of the ILs used in the calculations are summarized in Table 5.

**Table 5** Densities and viscosities of the ILs as a function of temperature

| IL | Density (g $m^{-3}$) and viscosity (mPa s) | Ref. |
|---|---|---|
| [emim][Ac] | $\rho = 10^{-3} \times (1280.8 - 0.608\,T)$<br>$\ln \mu = -1.657 + \frac{673.7}{(T - 196.1)}$ | [46] |
| [emim][DCA] | $\rho = 1.295 - 6.49 \times 10^{-4}\,T$<br>$\ln \mu = -1.719 + \frac{682.4}{(T - 143.7)}$ | [66] |
| [emim][$MeSO_4$] | $\rho = 10^{-3} \exp(7.331 - 6.1722 \times 10^{-4}T + 1.3862 * 10^{-7}T^2)$<br>$\ln \mu = -8.715 + \frac{814.37}{(T - 165.06)}$ | [42] |
| [emim][$EtSO_4$] | $\rho = 1.2541 - 5.98 \times 10^{-4}\,(T - 273.15)$<br>$\mu = 5.68 \times 10^{-3} T^{0.5} \exp\left(\frac{945}{T - 162}\right)$ | [67] |

A typical plot of the pressure decline in the gas phase with time for the absorption of $CO_2$ into four ILs at 313 K is shown in Figure 3. The pressures are normalized by their initial values at $t = 0$ to demonstrate the relative strength of each IL in the $CO_2$ absorption. The red diamonds show the measured pressures. The figure shows a comparatively very high strength for IL [emim][Ac] as the pressure stabilization time (equilibrium time) was about 6 h with a nearly 40 % drop in the initial gas pressure $P_0$ (bar). IL [emim][$MeSO_4$] showed relatively lower strength with 80 h of equilibrium time and a roughly 2 % drop in the initial gas pressure.

The solid curves of Figure 3 show the thin-film model (Model 1) prediction that was fitted to the data by tuning the diffusivity coefficient. The optimum values of the diffusivity coefficients that resulted in the best fit of Eq. 10 to the experimental data ($D_1$) are listed in Table . To find $D_1$, the experimental data within the range of $0 < t < t_1$ were used, where the values of $t_1$ are listed in Table 6. In all the calculations, the height of the liquid was taken as 0.708215297 cm. As shown in Figure , the pressures predicted by the thin-film model fairly agree with the measured pressures.

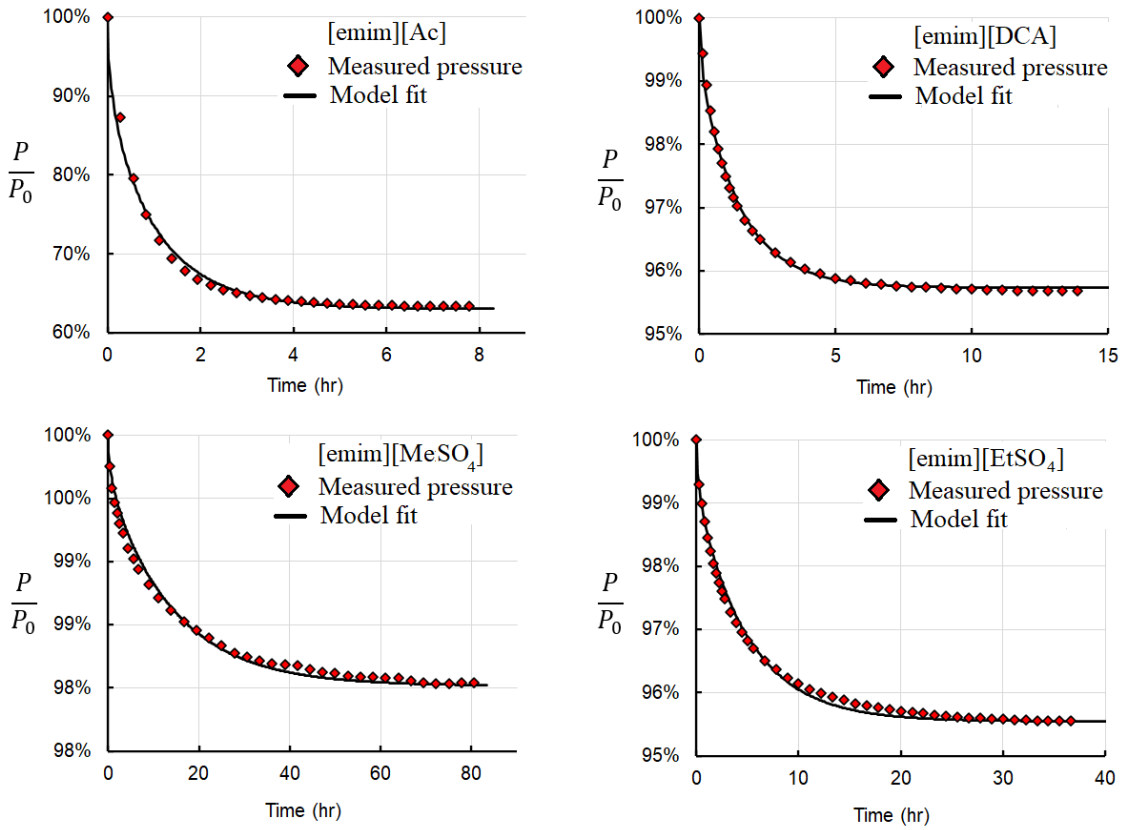


**Figure 3** Pressure decay in the gas phase in four typical experiments when the temperature is roughly 313 K (From Table 3). The red diamonds show the experimental data, and the solid curve shows the thin-film model (Model 1) predictions fitted to the data by tuning the diffusivity coefficient.

The diffusivity coefficients were also determined from the semi-infinite volume model ($D_2$) and the results are summarized in Table 6. To find $D_2$, the experimental data after 2 min and up to $t_2$ were used, where the values of $t_2$ are listed in Table 6.

The diffusivity coefficients developed in this work using the thin-film model (Model 1) and semi-infinite volume model (Model 2) are also compared with the data extracted from the correlations of Morgan et al. [40] and Hou and Baltus [41]. The correlation developed by Morgan et al. is based on the data from five imidazolium-based RTILs, considering the gas molar volume and the IL viscosity as the base parameters. The comparison between our data and the data obtained from this correlation is very relevant as the RTILs considered for this study are also imidazolium-based.

Morgan et al. [40] model was developed based on the data at $T$ = 303.15 K only. However, we used it for all temperatures to estimate the diffusion coefficient based on the proposed method. The Hou and Baltus [41] correlation is based on the data from RTILs at the temperature range of 283-323 K. This correlation includes important parameters such as viscosity, density, molecular weight, and temperature.

$D_{\mathrm{M}}$: Correlation proposed by Morgan et al.: $D_M = 2.66 \times 10^{-3} \mu_{\mathrm{IL}}^{-0.66} V_{\mathrm{A}}^{-1.04}$.

$D_{\mathrm{H}}$: Correlation proposed by Hou and Baltus: $D_H = 6.7 \times 10^{5}\ \mu_{\mathrm{IL}}^{-0.66} M_{\mathrm{IL}}^{-0.89} \rho_{\mathrm{IL}}^{4.8}\ T^{-3.3}$.

Where $\mu_{IL}$(cP), $V_A(\mathrm{cm^3.mol^{-1}})$, $M_{IL}$ $(\mathrm{g\,mol^{-1}})$, $\rho_{IL}(\mathrm{g\,cm^{-3}})$ and $T$(K) are the viscosity of the IL, molar volume of $CO_2$, the molecular weight of the IL, the density of the IL, and temperature, respectively.

**Table 6** Diffusion coefficients of $CO_2$ in different ILs

| IL | $T$ (K) | $P_0$ (bar) | $P_\infty$ (bar) | $t_1$ (min) | $t_2$ (min) | $D_1 \times 10^{10}$ ($m^2\ s^{-1}$) Model 1 | $D_2 \times 10^{10}$ ($m^2\ s^{-1}$) Model 2 | $SD$ $D_1$-$D_2$ | $D_{\mathrm{M}} \times 10^{10}$ ($m^2\ s^{-1}$) Morgan *et al.* | $D_{\mathrm{H}} \times 10^{10}$ ($m^2\ s^{-1}$) Hou & Baltus |
|---|---|---|---|---|---|---|---|---|---|---|
| **[emim][Ac]** | 303.1±0.05 | 2.596±0.003 | 1.343±0.001 | 4080 | 23 | 5.5±0.4 | 0.6±0.1 | 3.46 | 3.2 | 3.3 |
| | 302.1±0.05 | 3.582±0.004 | 2.104±0.002 | 4040 | 23 | 12.5±1.7 | 1.2±0.1 | 7.99 | 3.1 | 3.2 |
| | 313.2±0.05 | 3.558±0.004 | 2.254±0.002 | 2490 | 27 | 10.4±1.5 | 4.0±0.4 | 4.53 | 4.6 | 4.1 |
| | 323.2±0.05 | 3.555±0.004 | 2.385±0.002 | 2660 | 19 | 14.3±0.7 | 5.3±0.4 | 6.36 | 6.3 | 4.8 |
| | 333.2±0.05 | 3.583±0.004 | 2.523±0.003 | 1440 | 15 | 18.6±2.6 | 7.0±1.1 | 8.20 | 8.1 | 5.5 |
| **[emim][DCA]** | 303.6±0.05 | 2.166±0.002 | 2.073±0.002 | 550 | 18 | 19.1±2.3 | 13.9±1.4 | 3.68 | 12.9 | 12.5 |
| | 303.6±0.05 | 2.622±0.003 | 2.543±0.003 | 850 | 18 | 17.4±1.9 | 15.6±2.0 | 1.27 | 12.9 | 12.5 |
| | 303.2±0.05 | 3.603±0.004 | 3.483±0.003 | 720 | 20 | 18.8±2.6 | 19.2±2.3 | 0.28 | 3.3 | 3.2 |
| | 313.9±0.05 | 3.592±0.004 | 3.437±0.003 | 460 | 18 | 33.9±2.7 | 20.1±1.6 | 9.76 | 15.3 | 12.9 |
| | 322.7±0.05 | 3.590±0.004 | 3.501±0.004 | 330 | 25 | 26.9±2.7 | 27.1±2.7 | 0.14 | 17.4 | 13.1 |
| | 332.6±0.05 | 3.604±0.004 | 3.541±0.004 | 500 | 9 | 27.4±1.9 | 35.1±1.8 | 5.44 | 19.9 | 13.1 |
| **[emim][MeSO$_4$]** | 304.5±0.05 | 2.712±0.003 | 2.593±0.003 | 3800 | 11 | 2.6±0.1 | 9.3±1.3 | 4.74 | 4.6 | 7.6 |
| | 304.9±0.05 | 2.239±0.003 | 2.161±0.003 | 1030 | 10 | 2.3±0.3 | 7.7±0.8 | 3.82 | 4.6 | 7.6 |
| | 304.0±0.05 | 2.670±0.003 | 2.587±0.003 | 1060 | 10 | 2.5±0.2 | 7.2±0.5 | 3.32 | 4.5 | 7.5 |
| | 314.0±0.05 | 3.685±0.004 | 3.560±0.004 | 2300 | 6 | 5.7±0.5 | 12.6±0.8 | 4.88 | 5.8 | 8.4 |
| | 322.5±0.05 | 3.676±0.004 | 3.603±0.004 | 4000 | 10 | 4.1±0.3 | 18.2±1.8 | 9.97 | 7.0 | 9.1 |
| | 332.0±0.05 | 3.669±0.004 | 3.625±0.004 | 2560 | 17 | 5.4±0.7 | 23.3±2.8 | 12.66 | 8.5 | 9.8 |
| **[emim][EtSO$_4$]** | 303.9±0.05 | 2.689±0.003 | 2.555±0.003 | 1000 | 19 | 4.8±0.4 | 6.8±0.5 | 1.41 | 3.9 | 5.2 |
| | 303.1±0.05 | 3.691±0.004 | 3.470±0.003 | 800 | 10 | 6.8±0.8 | 8.2±0.9 | 0.99 | 3.8 | 5.1 |
| | 315.1±0.05 | 3.684±0.004 | 3.520±0.004 | 500 | 10 | 10.7±1.7 | 16.7±1.7 | 4.24 | 5.4 | 6.1 |
| | 324.4±0.05 | 3.704±0.004 | 3.562±0.004 | 500 | 26 | 11.4±1.5 | 21.5±2.8 | 7.14 | 6.7 | 6.8 |
| | 332.5±0.05 | 3.696±0.004 | 3.602±0.004 | 280 | 12 | 12.2±1.1 | 38.0±1.9 | 18.24 | 8.0 | 7.3 |

The diffusion coefficients presented in Table 6 show a considerable amount of difference between the values from the thin-film model (Model 1) and the semi-infinite volume model (Model 2). To understand the difference more easily, standard deviation (SD) values are listed in Table 6. In the current study, the change in the volume of the liquid due to the dissolution of $CO_2$ is neglected. To estimate the change in the liquid volume, a curve is fitted to the plot of volume change vs. mole fraction of $CO_2$ in the ILs provided in Aki et al. [68]:

$$\frac{\Delta V}{V_0} = 0.007738 - 0.02447\, x_{CO2} + 0.571292\, x_{CO2}^2$$

Using this equation, we found that the volume change for the experiments with [emim][DCA], [emim][MtSO4] and [emim][EtSO4] are smaller than 0.75%. For [emim] [AC], the volume change is nearly 3% due to a higher solubility. In this study, we ignore the effect of 3% volume change on the determined diffusivity coefficients.

For ILs [emim][Ac] and [emim][DCA], the semi-infinite volume model (Model 2) values are closer to the values from the correlations of Morgan et al. and Hou and Baltus. The thin-film model (Model 1) values for [emim] [$MeSO_4$] and [emim] [$EtSO_4$] are close to the one calculated from correlations of Morgan et al. [40] and Hou and Baltus [41]. We can presume that the thin-film model (Model 1) overestimates the diffusion coefficients of [emim][Ac] and [emim][DCA], while the semi-infinite volume model (Model 2) overestimates the diffusion coefficients of [emim][$MeSO_4$] and [emim][$EtSO_4$]. The validity of the assumption of the infinite liquid domain in model 2 was verified by inserting the calculated diffusivity coefficients ($D_2$) into eq. 11. For the assumption of a semi-infinite liquid domain to be valid, the concentration of $CO_2$ at the bottom of the pressure vessel at $t_2$ should be zero. For all experiments, C ($L$, $t_2$) was negligible except for [emim][DCA] at 322.7 K and [emim][$EtSO_4$] at 324.4 K in Table 6, which were found to be 1.3

and 0.7% of the interfacial concentration of $CO_2$ in the liquid, respectively, which are small enough to be ignored. The effect of temperature on the diffusion coefficients is very prominent in Table 6. An increase in the diffusion coefficients can be observed with an increase in temperature. For example, in the case of [emim][Ac], the model 1 diffusion coefficient has recorded an increase from $12.5 \times 10^{-10}$ to $18.6\times 10^{-10}$ $m^2$ $s^{-1}$ as the temperature rises from 302.1 to 333.2 K. For the same temperature increase, Model 2 diffusion coefficient has recorded an increase from $1.2 \times 10^{-10}$ to $7\times 10^{-10}$ $m^2$ $s^{-1}$. The increase in $CO_2$ diffusion coefficient with the increase in temperature has also been confirmed by other studies, reported in Table 7. There is not enough relevant $CO_2$ diffusion coefficient data available from the literature, except for the IL [emim][$EtSO_4$], from the studies of Wong et al. [69] and Jalili et al. [55]. It can be observed from Table 7 that the diffusion coefficients reported by Wong et al. [69] and Jalili et al. [55] are not quite comparable. The values reported by Wong et al. [69] are relatively very high. The [emim][$EtSO_4$] diffusion coefficients of this study (Table 6) are higher than the study of Jalili et al. [55] but lower than the one reported by Wong et al. [69].

**Table 7** Diffusivities of $CO_2$ in the studied ILs from different literature

| **ILs** | **T (K)** | $D \times 10^{10}$ **($m^2$ $s^{-1}$)** | **Ref.** |
|---|---|---|---|
| **[emim][Ac]** | 298.15 | 5.58 | [70] |
| **[emim][DCA]** | 298.15 | 11.60 | [9] |
| | 308.20 | 14.07 | [69] |
| | 318.20 | 17.06 | [69] |
| **[emim][$MeSO_4$]** | 298.15 | 3.88 | [9] |
| **[emim][$EtSO_4$]** | 303.20 | 10.36 | [69] |
| | 313.20 | 14.01 | [69] |
| | 323.20 | 16.41 | [69] |
| | 303.15 | 2.19 | [55] |
| | 323.15 | 5.08 | [55] |
| | 353.15 | 19.01 | [55] |

A visual comparison between the diffusivity coefficients obtained from Model 1 and Model 2 is provided in Figure 4. For [emim][Ac] and [emim][DCA], the diffusion coefficients predicted by the transient thin-film model are larger than those predicted by the semi-infinite volume model. However, for [emim][$MeSO_4$] and [emim][$EtSO_4$], the thin-film model predictions are smaller. Hou and Baltus [41] reported that the transient thin-film model produced more accurate results than the semi-infinite volume model. They attributed it to the way the Henry constant is calculated. In the transient thin-film model, the Henry constant is often determined by fitting the model predictions to the pressure decay data. In contrast, the Henry constant is calculated separately after each experiment in the semi-infinite volume model. In the current study, we calculated the Henry constant from the mass balance since our experiments were conducted long enough to make the pressure curve flat in each experiment. This means no further $CO_2$ diffused in the liquid, and equilibrium was reached.

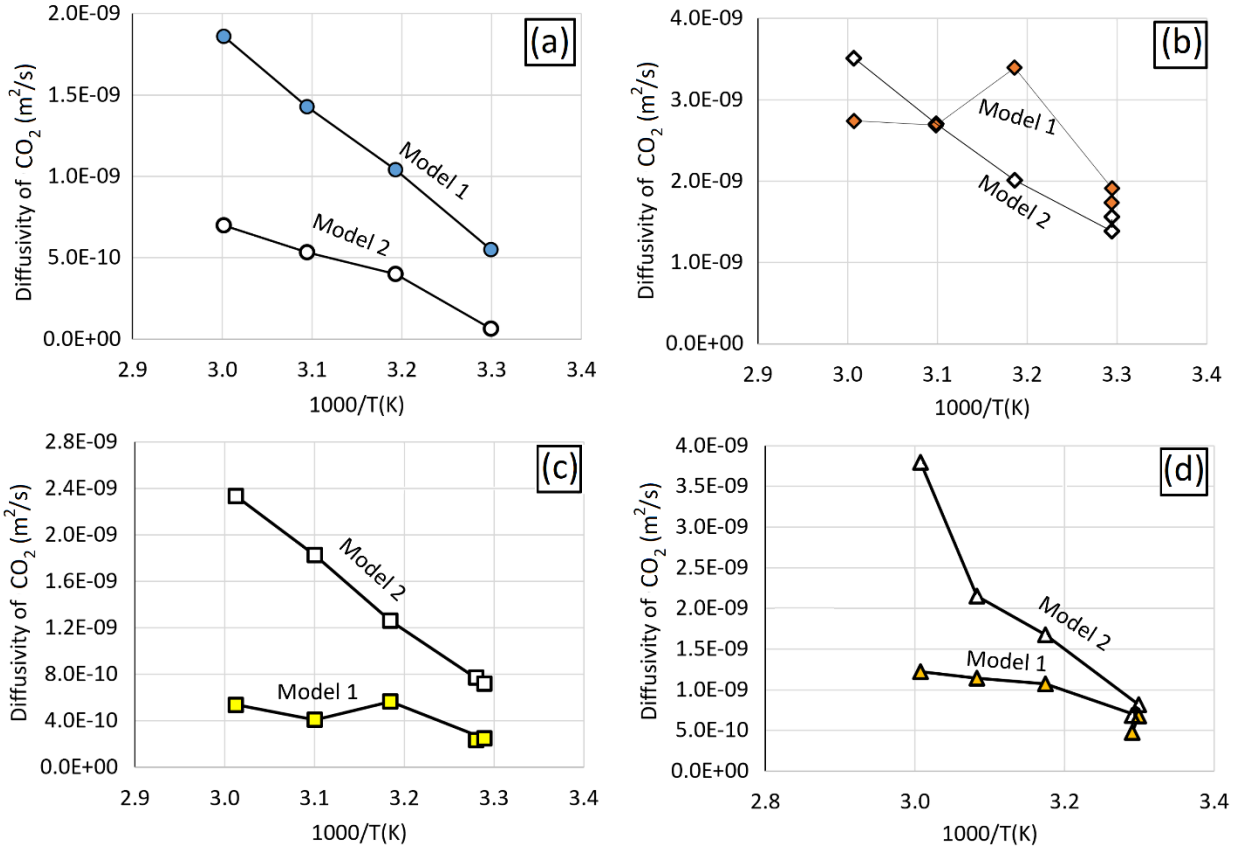


**Figure 4** The diffusion coefficients as a function of temperature calculated from models 1 and 2 for (a) [emim][Ac], (b) [emim][DCA], (c) [emim][$MeSO_4$], and (d) [emim][$EtSO_4$]. The colored data represent the predictions by model 1 (transient thin-film), and the open data show the predictions of model 2 (semi-infinite volume).

The diffusivity coefficients determined from the third model for the experiments at 313.15 K are demonstrated in Figure 5. For the typical experiment of diffusion in [emim][DCA], as seen in the second row in Figure 5, the diffusivity coefficient rapidly increases from nearly zero and reaches a maximum value of $4.3\times10^{-9}$ $m^2$/s after 2/3 h of the experiment. Then, it decreases moderately until it reaches a value of $2\times10^{-9}$ $m^2$/s at the end of the experiment. For this specific experiment, the optimum value obtained by the thin-film model is $3.4\times10^{-9}$ $m^2$/s, and that obtained by the semi-infinite volume model is $2\times10^{-9}$ $m^2$/s. Indeed, both values fall within the range of the predictions by the third model.

It is worth mentioning that the adjusted diffusivity coefficients obtained by the third model are not monotonous functions of time; they initially increase and then gradually decrease. Since the concentration of $CO_2$ in the liquid is increasing progressively, it can be said that the diffusivity coefficients increase with the concentration in the early stages of the diffusion processes. However, they show an inverse relation with the concentration after a certain time. This may address the ambiguity in the literature regarding the dependency of the diffusivity coefficient on the concentration. Based on our finding, $D$ could exhibit both behaviors; it is proportional to the concentration at the early stages of the diffusion, such as what could be seen within $0 < t < 2/3$ h in Figure 5(a), and is inversely proportional to the concentration after that, such as what could be seen at $t > 2/3$ h. Therefore, the anomaly in the diffusivity coefficient, which has been the subject of some papers in the literature and is explained by Hansen et al. [71] can be confirmed and may be addressed if it is taken to be a variable rather than a constant value. Here, we emphasize that the variable diffusivity coefficients in Figure 5 are not taken as a function of concentration. At each time step in the numerical solution, a constant $D$ throughout the whole domain was adjusted to fit the model prediction to the experimental data. Therefore, a comprehensive study is required to shed light on the diffusion coefficient's dependency on concentration.

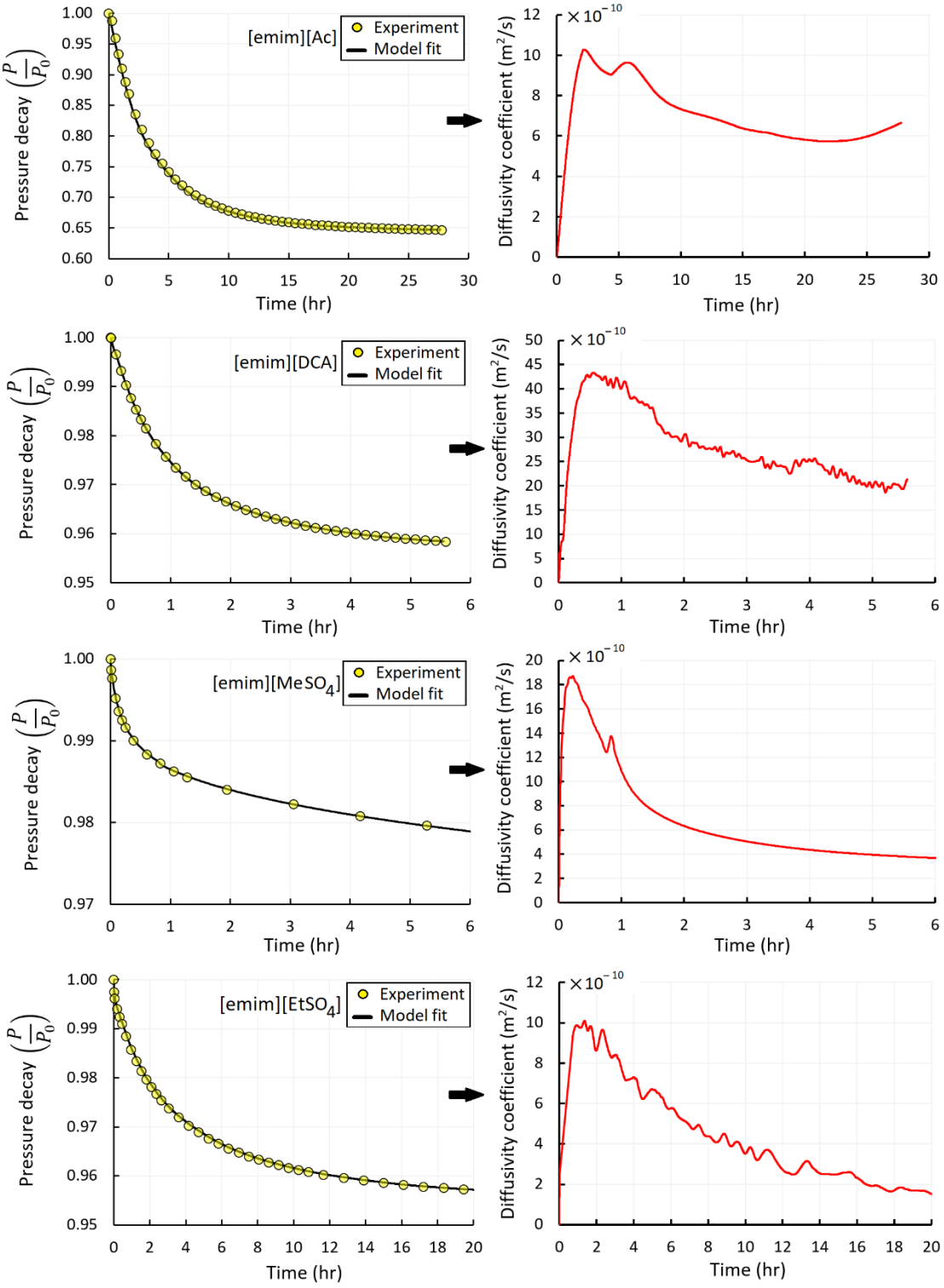


**Figure 5** Adjusted diffusivity coefficients for the experiments of the diffusion of $CO_2$ in four ILs at 313.15 K. The diffusivity coefficient in eq. 16 is adjusted so that the predicted pressures in the gas phase (left plots) match the measured ones.

Henry's law constant is temperature-dependent. The Henry constant as a function of the temperature for the ILs studied here may be expressed by a quadratic function as follows:

$$\ln(K_H/\text{bar}) = A_0 + A_1\left(\frac{1}{T}\right) + A_2\left(\frac{1}{T}\right)^2 \quad (19)$$

where $K_H$ (bar) is the Henry constant and $T$ (K) is the temperature. The coefficients of the quadratic function are listed in Table 8.

**Table 8** Coefficients of the quadratic function used to calculate the Henry constant

| IL | $A_2$ | $A_1$ | $A_0$ |
|---|---|---|---|
| [Emim][AC] | -4280352 | 25839.17 | -37.8926 |
| [Emim][DCA] | 1526846 | -10108.7 | 18.73385 |
| [Emim] [$MeSO_4$] | -3078378 | 18663.8 | -26.0861 |
| [Emim] [$EtSO_4$] | 5385315 | -35093.1 | 58.94063 |

The effect of temperature on $CO_2$ solubility in ILs can also be related to the Gibbs free energy ($\Delta_{sol}G^{\infty}$), enthalpy ($\Delta_{sol}H^{\infty}$), and entropy ($\Delta_{sol}S^{\infty}$) [41]. From the Henry constant, one may determine the change in the Gibbs free energy, enthalpy, and entropy of the system at a constant temperature when $CO_2$ diffuses into the liquid from the gas phase at the standard pressure to the standard state of infinite dilution in the liquid phase:

$$\Delta_{sol}G^{\infty} = RT\ln\left(\frac{K_H}{P^0}\right) \quad (20)$$

$$\Delta_{sol}H^{\infty} = -T^2\frac{\partial}{\partial T}\left(\frac{\Delta_{sol}G^{\infty}}{T}\right) = -RT^2\frac{\partial}{\partial T}\left[\ln\left(\frac{K_H}{P^0}\right)\right] \quad (21)$$

$$\Delta_{sol}S^{\infty} = \frac{\Delta_{sol}H^{\infty} - \Delta_{sol}G^{\infty}}{T} \quad (22)$$

The change in the Gibbs free energy, enthalpy, and entropy was calculated from Eqs. 20–22, and the results are listed in Table 9. It can be observed from Table 9 that the Gibbs free energy values are positive, presenting a non-spontaneous process. These values increased with an increase in

temperature. For example, for IL [emim][$EtSO_4$], the Gibbs free energy increased from 6.98 to 9.91 kJ $mol^{-1}$ by increasing the temperature from 303.14 to 332.51 K. The same phenomena were observed in other literature studies by Jacquemin et al. [72], Zhou et al. [73], and Shokouhi et al. [39]. Jacquemin et al., while studying Gibbs free energy for $CO_2$ dissolution in IL 1-butyl-3-methylimidazolium tetrafluoroborate ([bmim][$BF_4$]), reported values of 10.38, 12.87 kJ $mol^{-1}$ at temperatures of 303 and 333 K, respectively. For the same temperature increase, Shokouhi et al., while considering IL 1-(2-hydroxyethyl)-3-methylimidazolium tetrafluoroborate ([hemim][$BF_4$]), has reported an increase in the Gibbs free energy from 11.8 to14.1 kJ $mol^{-1}$. While comparing ILs of this study, it can be observed that the Gibbs free energy of the IL [emim][Ac] is lower than all other ILs. This can be linked with the very high $CO_2$ solubility of IL [emim][Ac] compared to other ILs of this study (Table 3). Enthalpy of $CO_2$ dissolution and entropy values were negative, which are presented in Table 9. The negative values of enthalpy indicate the strength of the favorable interaction between $CO_2$ and ILs. The decrease in the disorder of $CO_2$ and IL mixture can be observed from the negative values of entropy of dissolution. The enthalpy values of this work (for RTILs) mostly fall in the range of physical absorption (physisorption), which is -10 to -20 kJ $mol^{-1}$. For conventional amines (chemisorption), the enthalpy values fall in the range of -85 to -100 kJ $mol^{-1}$. The enthalpies of conventional amines are far higher than RTILs, but these high enthalpies bring very high expenses in the regeneration steps of amines. The interactions between $CO_2$ and RTILs consist of dispersion and polar (dipole−quadrupole) forces [65]. Moreover, the values of enthalpies and entropies are comparable to those reported in the literature. Zubeir et al. [65] reported an enthalpy of 13.68 kJ $mol^{-1}$ and entropy of 0.041 kJ $mol^{-1}$ $K^{-1}$ for RTIL 1-butyl-3-methylimidazolium tricyanomethanide ([bmim][tcm]). Blath et al., [24] reported an enthalpy of -12 kJ $mol^{-1}$ and entropy of -0.029 kJ $mol^{-1}$ $K^{-1}$, for the IL 1-Ethyl-3-methylimidazolium

bis(trifluoromethylsulfonyl)imide ([emim] [$NTf_2$]). The temperature has increased the magnitude of enthalpy and entropy of dissolution, as shown in Table 9. Similar effects of temperature were also confirmed for IL [bmim][$BF_4$] by Jacquemin et al. [72].

**Table 9** Thermodynamic properties of $CO_2$ in four ILs

| IL | $T$ (K) | $K_H$ (bar) | $\Delta_{sol}G^{\infty}$ (kJ mol$^{-1}$) | $\Delta_{sol}H^{\infty}$ (kJ mol$^{-1}$) | $\Delta_{sol}S^{\infty}$ (kJ mol$^{-1}$ K$^{-1}$) |
|---|---|---|---|---|---|
| **[emim][Ac]** | 303.1 | 5.7 | 1.99 | -12.21 | -0.063 |
| | 302.1 | 8.0 | 2.03 | -12.13 | -0.064 |
| | 313.2 | 10.0 | 2.68 | -13.03 | -0.054 |
| | 323.2 | 11.2 | 3.09 | -13.88 | -0.045 |
| | 333.2 | 12.9 | 3.56 | -14.75 | -0.038 |
| **[emim][DCA]** | 313.9 | 92.9 | 8.49 | -15.02 | -0.075 |
| | 322.7 | 136.0 | 9.75 | -15.87 | -0.079 |
| | 332.6 | 132.4 | 9.97 | -16.86 | -0.081 |
| **[emim][$MeSO_4$]** | 304.5 | 77.2 | 8.48 | -4.70 | -0.037 |
| | 304.9 | 128.2 | 9.81 | -4.72 | -0.042 |
| | 304.0 | 104.6 | 9.27 | -4.69 | -0.040 |
| | 314.0 | 112.5 | 8.92 | -5.00 | -0.043 |
| | 322.5 | 188.2 | 10.55 | -5.28 | -0.052 |
| | 332.0 | 149.0 | 10.22 | -5.59 | -0.054 |
| **[emim][$EtSO_4$]** | 303.9 | 59.9 | 7.84 | -14.05 | 0.033 |
| | 303.1 | 58.9 | 6.98 | -13.98 | 0.043 |
| | 315.1 | 68.8 | 7.67 | -15.11 | -0.062 |
| | 324.4 | 79.0 | 8.25 | -16.01 | -0.134 |
| | 332.5 | 133.1 | 9.91 | -16.82 | -0.193 |

## Conclusion

In this work, an experimental setup based on the isochoric pressure drop principle was developed to measure the solubility and binary diffusivity of four imidazolium cation-based RTILs, namely, [emim][Ac], [emim][DCA], [emim][$MeSO_4$], and [emim][$EtSO_4$]. Measurements were performed at low gas pressures, and parameter values were recorded under infinite dilution conditions. The molar fraction of $CO_2$ and Henry's law constant were measured from the experimental data. Constant and variable binary diffusion coefficients were calculated using the transient thin-film model, semi-infinite volume model, and variable diffusivity coefficient model. The variable

diffusivity coefficient model is a comparatively new approach to studying the concentration-based variations in the diffusion coefficients of $CO_2$ in RTILs.

$CO_2$ solubility and Henry's law constant strongly depended on the anion of IL. Based on these parameters the anions of [emim] cation can be ranked as $[Ac]^-$ >> $[EtSO_4]^-$ > $[DCA]^-$ > $[MeSO_4]^-$. In a typical experimental measurement for [emim][Ac] at 302.1 K, the $CO_2$ mole fraction was 0.26 with 8 bar Henry's law constant. An increase in temperature was recorded to have negatively affected the $CO_2$ solubility in RTILs. The standard deviations between diffusion coefficients of the thin-film and semi-infinite volume models indicate a considerable difference between the values obtained from both models. An increase in temperature seems to be significantly favorable for $CO_2$ diffusion coefficients. The variable diffusion coefficients from the third model were found not to be a monotonous function of time but rather a function of $CO_2$ concentration, which favors the diffusion coefficients in the early stages and shows an inverse relation after a certain time. The Gibbs free energy, enthalpy, and entropy values were found in the range of 1.99 to 10.55 kJ $mol^{-1}$, -4.69 to -16.82 kJ $mol^{-1}$, and -0.037 to -0.193 kJ $mol^{-1}$ $K^{-1}$, respectively. These thermodynamic parameters of $CO_2$ dissolution indicate the strength of the favorable interaction between $CO_2$ and RTILs, mildly exothermic in nature and falling in the range of physical absorption (physisorption).

## Nomenclature

| | |
|---|---|
| $\Delta_{\mathrm{sol}}G^{\infty}$ | Gibbs free energy |
| $\Delta_{\mathrm{sol}}H^{\infty}$ | Enthalpy |
| $\Delta_{\mathrm{sol}}S^{\infty}$ | Entropy |
| $A_0$, $A_1$, $A_2$ | Fitting parameters for Henry's constant |
| $D_1$ | Diffusion coefficient (model 1) |
| $D_2$ | Diffusion coefficient (model 2) |
| $D_{\mathrm{H}}$ | Diffusion coefficient (Hou and Baltus) |
| $D_{\mathrm{M}}$ | Diffusion coefficient (Morgan) |
| $K_H$ | Henry's law constant |
| $K_d$ | Derivative constant of the controller |
| $K_i$ | Integral constant of the controller |
| $K_p$ | Proportional constant of the controller |
| $M_{\mathrm{IL}}$ | Molar mass of the ionic liquid |
| $P$ | Instantaneous gas pressure in the chamber |
| $V_{\mathrm{IL}}$ | Volume of the ionic liquid |
| $n_{IL}$ | the number of moles of IL |
| $n_{CO2}$ | Molar amount of $CO_2$ gas absorbed at equilibrium |
| $x_{\mathrm{CO2}}$ | Solubility of $CO_2$ (molar fraction) |
| $\rho_{\mathrm{IL}}$ | Density of the ionic liquid |
| $P_0$ | Initial pressure |
| $P_{\infty}$ | Equilibrium state pressure |
| $D$ | Diffusion coefficient |
| $L$ | Thickness of the ionic liquid film |
| $N$ | Number of moles of $CO_2$ in the gas |
| $R$ | Gas constant |
| $T$ | Temperature |
| $V$ | Volume of the gas |
| $c$ | Concentration |
| $e$ | Error |
| $k$ | Fitting parameter for model 2 |
| $t$ | Time |
| $x$ | Spatial coordinate |
| $z$ | Spatial coordinate |
| $\mu$ | Viscosity |

## References


[1] M. Younas, T. Tahir, C. Wu, S. Farrukh, Q. Sohaib, A. Muhammad, M. Rezakazemi, J. Li, Post-combustion CO 2 capture with sweep gas in thin fi lm composite ( TFC ) hollow fi ber membrane ( HFM ) contactor, Journal of CO2 Utilization. 40 (2020) 101266. https://doi.org/10.1016/j.jcou.2020.101266.

[2] I.K. Swati, Q. Sohaib, S. Cao, M. Younas, D. Liu, J. Gui, M. Rezakazemi, Protic/aprotic ionic liquids for effective CO2 separation using supported ionic liquid membrane, Chemosphere. 267 (2021) 128894. https://doi.org/10.1016/j.chemosphere.2020.128894.

[3] J.D. Figueroa, T. Fout, S. Plasynski, H. McIlvried, R.D. Srivastava, Advances in CO2 capture technology-The U.S. Department of Energy's Carbon Sequestration Program, International Journal of Greenhouse Gas Control. (2008). https://doi.org/10.1016/S1750-5836(07)00094-1.
[4] L. Zhou, J. Fan, X. Shang, J. Wang, Solubilities of CO2, H2, N2 and O 2 in ionic liquid 1-n-butyl-3-methylimidazolium heptafluorobutyrate, Journal of Chemical Thermodynamics. 59 (2013) 28–34. https://doi.org/10.1016/j.jct.2012.11.030.
[5] A. Henni, J. Li, P. Tontiwachwuthikul, Reaction kinetics of CO2 in aqueous 1-amino-2-propanol, 3-amino-1-propanol, and dimethylmonoethanolamine solutions in the temperature range of 298-313 K using the stopped-flow technique, Industrial and Engineering Chemistry Research. 47 (2008) 2213–2220. https://doi.org/10.1021/ie070587r.
[6] S. Qazi, L. Gómez-coma, J. Albo, S. Druon-bocquet, A. Irabien, CO 2 capture in a hollow fiber membrane contactor coupled with ionic liquid : Influence of membrane wetting and process parameters, Separation and Purification Technology. 233 (2020) 115986. https://doi.org/10.1016/j.seppur.2019.115986.
[7] Z. Dai, R.D. Noble, D.L. Gin, X. Zhang, L. Deng, Combination of ionic liquids with membrane technology: A new approach for CO2separation, Journal of Membrane Science. 497 (2016) 1–20. https://doi.org/10.1016/j.memsci.2015.08.060.
[8] S. Qazi, L. Gómez-Coma, J. Albo, S. Druon-Bocquet, A. Irabien, M. Younas, J. Sanchez-Marcano, Mathematical modeling of CO 2 absorption with ionic liquids in a membrane contactor, study of absorption kinetics and influence of temperature, Journal of Chemical Technology & Biotechnology. (2019) jctb.6265. https://doi.org/10.1002/jctb.6265.
[9] S. Qazi, J. Manuel Vadillo, L. Gómez-Coma, J. Albo, S. Druon-Bocquet, A. Irabien, J. Sanchez-Marcano, CO2 Capture with Room Temperature Ionic Liquids; Coupled Absorption/Desorption and Single Module Absorption in Membrane Contactor, Chemical Engineering Science. (2020). https://doi.org/10.1016/j.ces.2020.115719.
[10] Q. Sohaib, J.M. Vadillo, L. Gómez-Coma, J. Albo, S. Druon-Bocquet, A. Irabien, J. Sanchez-Marcano, Post-combustion CO2 capture by coupling [emim] cation based ionic liquids with a membrane contactor; Pseudo-steady-state approach, International Journal of Greenhouse Gas Control. (2020). https://doi.org/10.1016/j.ijggc.2020.103076.
[11] Q. Sohaib, A. Muhammad, M. Younas, M. Rezakazemi, S. Druon-Bocquet, J. Sanchez-Marcano, Rigorous non-isothermal modeling approach for mass and energy transport during CO2 absorption into aqueous solution of amino acid ionic liquids in hollow fiber membrane contactors, Separation and Purification Technology. (2021). https://doi.org/10.1016/j.seppur.2020.117644.
[12] Q. Sohaib, Post-combustion Carbon Dioxide Capture By Coupling Ionic Liquids With Membrane Contactors: Experimental, Modeling And Simulation, Université de Montpellier, 2020.
[13] M.B. Shiflett, A. Yokozeki, Phase behavior of carbon dioxide in ionic liquids: [emim][acetate], [emim][trifluoroacetate], and [emim][acetate] + [emim][trifluoroacetate] mixtures, Journal of Chemical and Engineering Data. 54 (2009) 108–114. https://doi.org/10.1021/je800701j.
[14] M. Ramdin, T.W. De Loos, T.J.H. Vlugt, State-of-the-art of CO \n 2 capture with ionic liquids, Industrial and Engineering Chemistry Research. 51 (2012) 8149–8177. https://doi.org/10.1021/ie3003705.
[15] S.N.V.K. Aki, B.R. Mellein, E.M. Saurer, J.F. Brennecke, High-pressure phase behavior of carbon dioxide with imidazolium-based ionic liquids, Journal of Physical Chemistry B. (2004). https://doi.org/10.1021/jp046895+.
[16] J.L. Anthony, J.L. Anderson, E.J. Maginn, J.F. Brennecke, Anion Effects on Gas Solubility in Ionic Liquids, The Journal of Physical Chemistry B. (2005). https://doi.org/10.1021/jp046404l.

[17] C. Cadena, J.L. Anthony, J.K. Shah, T.I. Morrow, J.F. Brennecke, E.J. Maginn, Why is CO2 so Soluble in Imidazolium-Based Ionic Liquids?, Journal of the American Chemical Society. (2004). https://doi.org/10.1021/ja039615x.
[18] L.A. Blanchard, Z. Gu, J.F. Brennecke, High-pressure phase behavior of ionic liquid/CO2 systems, Journal of Physical Chemistry B. (2001). https://doi.org/10.1021/jp003309d.
[19] S.G. Kazarian, B.J. Briscoe, T. Welton, Combining ionic liquids and supercritical fluids: In situ ATR-IR study of CO2 dissolved in two ionic liquids at high pressures, Chemical Communications. (2000). https://doi.org/10.1039/b005514j.
[20] C. Wang, H. Luo, D.E. Jiang, H. Li, S. Dai, Carbon dioxide capture by superbase-derived protic ionic liquids, Angewandte Chemie - International Edition. (2010). https://doi.org/10.1002/anie.201002641.
[21] S. Ren, Y. Hou, W. Wu, S. Tian, W. Liu, CO 2 capture from flue gas at high temperatures by new ionic liquids with high capacity, RSC Advances. (2012). https://doi.org/10.1039/c2ra00996j.
[22] H. Ohno, K. Fukumoto, Amino acid ionic liquids, Accounts of Chemical Research. (2007). https://doi.org/10.1021/ar700053z.
[23] A.H. Jalili, A. Mehdizadeh, M. Shokouhi, A.N. Ahmadi, M. Hosseini-Jenab, F. Fateminassab, Solubility and diffusion of CO2and H2S in the ionic liquid 1-ethyl-3-methylimidazolium ethylsulfate, Journal of Chemical Thermodynamics. 42 (2010) 1298–1303. https://doi.org/10.1016/j.jct.2010.05.008.
[24] J. Blath, M. Christ, N. Deubler, T. Hirth, T. Schiestel, Gas solubilities in room temperature ionic liquids - Correlation between RTiL-molar mass and Henry's law constant, Chemical Engineering Journal. (2011). https://doi.org/10.1016/j.cej.2011.05.084.
[25] C.A. Ohlin, P.J. Dyson, G. Laurenczy, E. Polytechnique, C.- Lausanne, Carbon monoxide solubility in ionic liquids : determination , prediction and relevance to hydroformylation †, (2004) 1070–1071.
[26] J. Kumełan, D. Tuma, Á.L.P.S. Kamps, G. Maurer, Solubility of the single gases carbon dioxide and hydrogen in the ionic liquid [bmpy][Tf2N], Journal of Chemical and Engineering Data. (2010). https://doi.org/10.1021/je900298e.
[27] R. Condemarin, P. Scovazzo, Gas permeabilities , solubilities , diffusivities , and diffusivity correlations for ammonium-based room temperature ionic liquids with comparison to imidazolium and phosphonium RTIL data, 147 (2009) 51–57. https://doi.org/10.1016/j.cej.2008.11.015.
[28] J.E. Bara, T.K. Carlisle, C.J. Gabriel, D. Camper, A. Finotello, D.L. Gin, R.D. Noble, Guide to CO 2 Separations in Imidazolium-Based Room-Temperature Ionic Liquids, (2009) 2739–2751.
[29] M. Shokouhi, M. Adibi, A.H. Jalili, M. Hosseini-Jenab, A. Mehdizadeh, Solubility and diffusion of H2S and CO2 in the ionic liquid 1-(2-Hydroxyethyl)-3-methylimidazolium tetrafluoroborate, Journal of Chemical and Engineering Data. (2010). https://doi.org/10.1021/je900716q.
[30] J. Blath, N. Deubler, T. Hirth, T. Schiestel, Chemisorption of carbon dioxide in imidazolium based ionic liquids with carboxylic anions, Chemical Engineering Journal. 181–182 (2012) 152–158. https://doi.org/10.1016/j.cej.2011.11.042.
[31] Z. Yang, S. Bryant, M. Dong, An Analytical Method of Estimating Diffusion Coef fi cients of Gases in Liquids from Pressure Decay Tests, 65 (2019) 434–445. https://doi.org/10.1002/aic.16408.
[32] Z. Yang, M. Dong, H. Gong, Y. Li, Determination of Mass Transfer Coe ffi cient of Methane in Heavy Oil- Saturated Unconsolidated Porous Media Using Constant-Pressure Technique, (2017). https://doi.org/10.1021/acs.iecr.7b01088.
[33] S.R. Etminan, B.B. Maini, Z. Chen, Determination of mass transfer parameters in solvent-based oil recovery techniques using a non-equilibrium boundary condition at the interface, FUEL. 120 (2014) 218–232. https://doi.org/10.1016/j.fuel.2013.11.027.

[34] R. Rakoczy, J. Lechowska, M. Kordas, M. Konopacki, K. Fijałkowski, Effects of a rotating magnetic field on gas-liquid mass transfer coefficient, 327 (2017) 608–617. https://doi.org/10.1016/j.cej.2017.06.132.
[35] A. Sell, H. Fadaei, M. Kim, D. Sinton, Micro fl uidic Approach for Reservoir-Speci fi c Analysis, (2013).
[36] P. Taylor, X. Zhang, J.M. Shaw, Petroleum Science and Technology Liquid-phase Mutual Diffusion Coefficients for Heavy Oil + Light Hydrocarbon Mixtures Liquid-phase Mutual Diffusion Coefficients for, (2007) 37–41. https://doi.org/10.1080/10916460500411796.
[37] C. Yang, Y. Gu, U. Regina, A New Method for Measuring Solvent Pendant Drop Shape Analysis ( DPDSA ), (2006) 5–8.
[38] W. Afzal, X. Liu, J.M. Prausnitz, Solubilities of some gases in four immidazolium-based ionic liquids, The Journal of Chemical Thermodynamics. 63 (2013) 88–94. https://doi.org/10.1016/j.jct.2013.03.007.
[39] M. Shokouhi, M. Adibi, A.H. Jalili, M. Hosseini-jenab, A. Mehdizadeh, Mohammad Shokouhi, Mina Adibi, Amir Hossein Jalili,* Masih Hosseini-Jenab, and Ali Mehdizadeh, 87 (2010) 1663–1668.
[40] D. Morgan, L. Ferguson, P. Scovazzo, Diffusivities of gases in room-temperature ionic Liquids: Data and correlations obtained using a lag-time technique, Industrial and Engineering Chemistry Research. 44 (2005) 4815–4823. https://doi.org/10.1021/ie048825v.
[41] H. Ying, R.E. Baltus, Experimental measurement of the solubility and diffusivity of CO 2 in room-temperature ionic liquids using a transient thin-liquid-film method, Industrial and Engineering Chemistry Research. (2007). https://doi.org/10.1021/ie070501u.
[42] A.J.L. Costa, M.S.S. Esperanca, I.M. Marrucho, L.P.N. Rebelo, Densities and Viscosities of 1-Ethyl-3-methylimidazolium n -Alkyl Sulfates, J. Chem. Eng. Data. 56 (2011) 3433–3441.
[43] J. Klomfar, M. Součková, J. Pátek, Temperature dependence of the surface tension and density at 0.1 MPa for 1-ethyl- and 1-butyl-3-methylimidazolium dicyanamide, Journal of Chemical and Engineering Data. (2011). https://doi.org/10.1021/je200502j.
[44] M. Larriba, P. Navarro, J. García, F. Rodríguez, Liquid-liquid extraction of toluene from heptane using [emim][DCA], [bmim][DCA], and [emim][TCM] ionic liquids, Industrial and Engineering Chemistry Research. 52 (2013) 2714–2720. https://doi.org/10.1021/ie303357s.
[45] E. Gómez, B. González, N. Calvar, E. Tojo, Á. Domínguez, Physical Properties of Pure 1-Ethyl-3-methylimidazolium Ethylsulfate and Its Binary Mixtures with Ethanol and Water at Several Temperatures, Journal of Chemical & Engineering Data. 51 (2006) 2096–2102. https://doi.org/10.1021/je060228n.
[46] A. Nazet, S. Sokolov, T. Sonnleitner, T. Makino, M. Kanakubo, R. Buchner, Densities, Viscosities, and Conductivities of the Imidazolium Ionic Liquids [Emim][Ac], [Emim][FAP], [Bmim][BETI], [Bmim][FSI], [Hmim][TFSI], and [Omim][TFSI], Journal of Chemical and Engineering Data. 60 (2015) 2400–2411. https://doi.org/10.1021/acs.jced.5b00285.
[47] A.P. Fröba, H. Kremer, A. Leipertz, Density, Refractive Index, Interfacial Tension, and Viscosity of Ionic Liquids [EMIM][EtSO $_4$ ], [EMIM][NTf $_2$ ], [EMIM][N(CN) $_2$ ], and [OMA][NTf $_2$ ] in Dependence on Temperature at Atmospheric Pressure, J. Phys. Chem. B. 112 (2008) 12420–12430. https://doi.org/10.1021/jp804319a.
[48] J.-Y. Wang, F.-Y. Zhao, Y.-M. Liu, X.-L. Wang, Y.-Q. Hu, Thermophysical properties of pure 1-ethyl-3-methylimidazolium methylsulphate and its binary mixtures with alcohols, Fluid Phase Equilibria. 305 (2011) 114–120. https://doi.org/10.1016/j.fluid.2011.03.008.
[49] H.F.D. Almeida, A.R.R. Teles, J.A. Lopes-da-Silva, M.G. Freire, J.A.P. Coutinho, Influence of the anion on the surface tension of 1-ethyl-3-methylimidazolium-based ionic liquids, The Journal of Chemical Thermodynamics. 54 (2012) 49–54. https://doi.org/10.1016/j.jct.2012.03.008.

[50] E. Rilo, M. Domínguez-Pérez, J. Vila, L.M. Varela, O. Cabeza, Surface tension of four binary systems containing (1-ethyl-3-methyl imidazolium alkyl sulphate ionic liquid+water or + ethanol), The Journal of Chemical Thermodynamics. 49 (2012) 165–171. https://doi.org/10.1016/j.jct.2012.01.023.
[51] W. Martino, J.F. de la Mora, Y. Yoshida, G. Saito, J. Wilkes, Surface tension measurements of highly conducting ionic liquids, Green Chem. 8 (2006) 390. https://doi.org/10.1039/b515404a.
[52] M.S. AlTuwaim, A.S. Al-Jimaz, K.H.A.E. Alkhaldi, Effect of the Alkyl Chain on the Physical Properties of Imidazolium-Based Ionic Liquids with 1-Propanol, 1-Butanol, and 1-Pentanol Binary Mixtures, J. Chem. Eng. Data. 64 (2019) 1366–1377. https://doi.org/10.1021/acs.jced.8b00948.
[53] M.B. Shiflett, A. Yokozeki, Solubilities and diffusivities of carbon dioxide in ionic liquids: [bmim][PF6] and [bmim][BF4], Industrial and Engineering Chemistry Research. (2005). https://doi.org/10.1021/ie058003d.
[54] Z. Lei, C. Dai, B. Chen, Gas solubility in ionic liquids, Chemical Reviews. (2014). https://doi.org/10.1021/cr300497a.
[55] A.H. Jalili, A. Mehdizadeh, M. Shokouhi, A.N. Ahmadi, M. Hosseini-Jenab, F. Fateminassab, Solubility and diffusion of CO2 and H2S in the ionic liquid 1-ethyl-3-methylimidazolium ethylsulfate, The Journal of Chemical Thermodynamics. 42 (2010) 1298–1303. https://doi.org/10.1016/j.jct.2010.05.008.
[56] A.N. Soriano, B.T. Doma, M.-H. Li, Carbon dioxide solubility in some ionic liquids at moderate pressures, Journal of the Taiwan Institute of Chemical Engineers. 40 (2009) 387–393. https://doi.org/10.1016/j.jtice.2008.12.002.
[57] F. Zareiekordshouli, A. Lashanizadehgan, P. Darvishi, Experimental and theoretical study of CO2 solubility under high pressure conditions in the ionic liquid 1-ethyl-3-methylimidazolium acetate, The Journal of Supercritical Fluids. 133 (2018) 195–210. https://doi.org/10.1016/j.supflu.2017.10.008.
[58] J. Blath, N. Deubler, T. Hirth, T. Schiestel, Chemisorption of carbon dioxide in imidazolium based ionic liquids with carboxylic anions, Chemical Engineering Journal. 181–182 (2012) 152–158. https://doi.org/10.1016/j.cej.2011.11.042.
[59] K. Huang, H.-L. Peng, Solubilities of Carbon Dioxide in 1-Ethyl-3-methylimidazolium Thiocyanate, 1-Ethyl-3-methylimidazolium Dicyanamide, and 1-Ethyl-3-methylimidazolium Tricyanomethanide at (298.2 to 373.2) K and (0 to 300.0) kPa, J. Chem. Eng. Data. 62 (2017) 4108–4116. https://doi.org/10.1021/acs.jced.7b00476.
[60] D. Camper, C. Becker, C. Koval, R. Noble, Low Pressure Hydrocarbon Solubility in Room Temperature Ionic Liquids Containing Imidazolium Rings Interpreted Using Regular Solution Theory, Ind. Eng. Chem. Res. 44 (2005) 1928–1933. https://doi.org/10.1021/ie049312r.
[61] J.-H. Yim, S.-J. Ha, J.S. Lim, Measurement and Correlation of $CO_2$ Solubility in 1-Ethyl-3-methylimidazolium ([EMIM]) Cation-Based Ionic Liquids: [EMIM][Ac], [EMIM][Cl], and [EMIM][$MeSO_4$], J. Chem. Eng. Data. 63 (2018) 508–518. https://doi.org/10.1021/acs.jced.7b00532.
[62] A. Finotello, J.E. Bara, D. Camper, R.D. Noble, Room-Temperature Ionic Liquids: Temperature Dependence of Gas Solubility Selectivity, Ind. Eng. Chem. Res. 47 (2008) 3453–3459. https://doi.org/10.1021/ie0704142.
[63] G. Wang, W. Hou, F. Xiao, J. Geng, Y. Wu, Z. Zhang, Low viscosity triethylbutylammonium acetate as a task-specific ionic liquid for reversible CO2 absorption, Journal of Chemical and Engineering Data. 56 (2011) 1125–1133. https://doi.org/10.1021/je101014q.
[64] A. Yokozeki, B. Shiflett Mark, P. Junk Christopher, M. Grieco Liane, T. Foo, Physical and chemical absorptions of carbon dioxide in room-temperature ionic liquids, The Journal of Physical Chemistry. B. 112 (2008) 16654–16663.

[65] L.F. Zubeir, G.E. Romanos, W.M.A. Weggemans, B. Iliev, T.J.S. Schubert, M.C. Kroon, Solubility and Diffusivity of CO<inf>2</inf> in the Ionic Liquid 1-Butyl-3-methylimidazolium Tricyanomethanide within a Large Pressure Range (0.01 MPa to 10 MPa), Journal of Chemical and Engineering Data. 60 (2015) 1544–1562. https://doi.org/10.1021/je500765m.
[66] E. Quijada-Maldonado, S. Van Der Boogaart, J.H. Lijbers, G.W. Meindersma, A.B. De Haan, Experimental densities, dynamic viscosities and surface tensions of the ionic liquids series 1-ethyl-3-methylimidazolium acetate and dicyanamide and their binary and ternary mixtures with water and ethanol at T = (298.15 to 343.15 K), Journal of Chemical Thermodynamics. 51 (2012) 51–58. https://doi.org/10.1016/j.jct.2012.02.027.
[67] J. Jacquemin, P. Husson, A.A.H. Padua, V. Majer, Density and viscosity of several pure and water-saturated ionic liquids, Green Chem. 8 (2006) 172–180. https://doi.org/10.1039/B513231B.
[68] S.N.V.K. Aki, B.R. Mellein, E.M. Saurer, J.F. Brennecke, High-Pressure Phase Behavior of Carbon Dioxide with Imidazolium-Based Ionic Liquids, J. Phys. Chem. B. 108 (2004) 20355–20365. https://doi.org/10.1021/jp046895+.
[69] C.-L. Wong, A.N. Soriano, M.-H. Li, Diffusion coefficients and molar conductivities in aqueous solutions of 1-ethyl-3-methylimidazolium-based ionic liquids, Fluid Phase Equilibria. 271 (2008) 43–52. https://doi.org/10.1016/j.fluid.2008.07.006.
[70] J.M. Vadillo, L. Gómez-Coma, A. Garea, A. Irabien, CO2 Desorption Performance from Imidazolium Ionic Liquids by Membrane Vacuum Regeneration Technology, Membranes. 10 (2020) 234. https://doi.org/10.3390/membranes10090234.
[71] A. Hansen, E.G. Flekkøy, B. Baldelli, Anomalous Diffusion in Systems with Concentration-Dependent Diffusivity: Exact Solutions and Particle Simulations, Frontiers in Physics. (2020). https://doi.org/10.3389/fphy.2020.519624.
[72] J. Jacquemin, M.F. Costa Gomes, P. Husson, V. Majer, Solubility of carbon dioxide, ethane, methane, oxygen, nitrogen, hydrogen, argon, and carbon monoxide in 1-butyl-3-methylimidazolium tetrafluoroborate between temperatures 283 K and 343 K and at pressures close to atmospheric, Journal of Chemical Thermodynamics. (2006). https://doi.org/10.1016/j.jct.2005.07.002.
[73] L. Zhou, J. Fan, X. Shang, J. Wang, Solubilities of CO2, H2, N2 and O 2 in ionic liquid 1-n-butyl-3-methylimidazolium heptafluorobutyrate, Journal of Chemical Thermodynamics. 59 (2013) 28–34. https://doi.org/10.1016/j.jct.2012.11.030.